AD-756 236

Effect of Microstructure and Environmment on Stress Corrosion of 7075 Aluminum Alloy

Grumman Aerospace Corp.

JANUARY 1973

RM-5643

EFFECT OF MICROSTRUCTURE AND ENVIRONMENT ON STRESS CORROSION OF 7075 ALUMINUM ALLOY

January 1973

Grumman Research Department Memorandum RM-564J

EFFECT OF MICROSTRUCTURE AND ENVIRONMENT ON STRESS CORROSION OF 7075 ALUMINUM ALLOY[+]

by

G. Geschwind and P. N. Adler

Materials and Structural Mechanics

January 1973

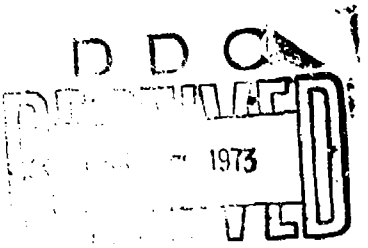

[+]To be presented at Corrosion/'73 at Anaheim, California, in March 1973.

Approved by:

Charles E. Mack, Jr.
Director of Research

U

Security Classification

DOCUMENT CONTROL DATA - R & D

(Security classification of title, body of abstract and indexing annotation must be entered when the overall report is classified)

1. ORIGINATING ACTIVITY (Corporate author)	2a. REPORT SECURITY CLASSIFICATION
Grumman Aerospace Corporation	U
	2b. GROUP

3. REPORT TITLE

Effect of Microstructure and Environment on Stress Corrosion of 7075 Aluminum Alloy

4. DESCRIPTIVE NOTES (Type of report and inclusive dates)

Research Report

5. AUTHOR(S) (First name, middle initial, last name)

G. Geschwind and P. N. Adler

6. REPORT DATE	7a. TOTAL NO. OF PAGES	7b. NO. OF REFS
January 1973	26	14

8a. CONTRACT OR GRANT NO.	9a. ORIGINATOR'S REPORT NUMBER(S)
b. PROJECT NO.	RM-564J
c. N/A	9b. OTHER REPORT NO(S) (Any other numbers that may be assigned this report)
d.	N/A

10. DISTRIBUTION STATEMENT

Approved for public release, distribution unlimited.

11. SUPPLEMENTARY NOTES	12. SPONSORING MILITARY ACTIVITY

13. ABSTRACT

Grain boundary microstructure as well as the pH in a chloride ion solution environment has been found to be significant to stress corrosion attack in 7075 aluminum alloys. The influence of these factors on both the intiiation and propagation of cracking and themode of attack in these alloys will be described. Microstructural modifications to attain desirable stress corrosion resistance will be suggested.

DD FORM 1 NOV 65 1473

II

U

Security Classification

EFFECT OF MICROSTRUCTURE AND ENVIRONMENT ON STRESS CORROSION OF 7075 ALUMINUM ALLOY

G. Geschwind and P. N. Adler
Grumman Aerospace Corporation
Bethpage, New York 11714

Introduction

In previous work (Ref. 1), we have reported that the stress-corrosion susceptibility of highest strength 7075 aluminum alloy is dependent upon grain boundary precipitate interparticle spacing (d) and the pH in an aqueous chloride environment. Comparison of the failure times (TTF) at a pH = 3.0, approximately that found adjacent to crack tips in 7075 (Ref. 2, 3), indicated a linear relation between log TTF and the grain boundary interparticle spacing (d). This supports earlier work suggesting the importance of grain boundary precipitate structure to stress corrosion susceptibility in this type alloy (Ref. 4, 5, 6). One of the interesting observations in our previous study concerns the change in susceptibility as a function of pH over the 0.7 to 2.0 range for two of the three grain boundary microstructures examined. Other investigators (Ref. 7, 8) did not find the susceptibility to be dependent on pH over a 1.0 to 6.2 pH range for a similar Al-Mg-Zn alloy in a comparable environment, although they did observe pH dependent differences in initial crack propagation rates. An anodic dissolution mechanism and local pH variation within the cracks were suggested to account for their observations.

The present work proposes a mechanism of stress corrosion attack based on both anodic dissolution and stress concentration at grain boundary precipitate particles. Earlier results and the TTF-pH characteristics of non-stress corrosion susceptible, overaged 7075-T7351 are considered as well as the attack morphology associated with test exposure.

Materials and Experimental Details

All the specimens used in this study were prepared from commercial material having chemical compositions within the specified limits for the 7075 alloy (Ref. 9). Both highest strength T651 and overaged T7351 bar stock were used. Details of the specimen size and geometry have been reported previously (Ref. 10). All specimens were cut so that the short transverse direction was parallel to the direction of loading thus insuring maximum susceptibility (Ref. 11). In addition to the as-received (AR) T651 and T7351 conditions, two heat treatments were used to vary grain boundary microstructure while maintaining constant matrix microstructure. In one, specimens of AR T651 were solution treated at 490°C for two hours in a flowing argon atmosphere, quenched into water at 20°C, then aged in a silicone oil bath at 120°C for 24 hours. These specimens were identified as water quenched (WQ) material. In the other treatment, specimens were solution treated for two hours in flowing argon, quenched into liquid nitrogen and aged at 120°C for 48 hours. These specimens were identified as liquid nitrogen quenched (LNQ) material. Table I lists the microstructural features of importance for these samples.

Stress-corrosion testing was conducted in a specially constructed apparatus in which a specimen is maintained under load while exposed to a continuously circulating corrosive solution. An initial stress of 30,000 psi, which is approximately 45% of the reported yield stresses for these materials, was used throughout. The load was continuously monitored by a resistance type strain gauge and the specimen extension by a linear variable differential transformer (LVDT) type strain gauge with a sensitivity of $\pm$ 2 x 10^{-6} inches. A method for the analysis of the extension-time behavior has been reported (Ref. 12).

The test solution was contained in a sealed oxygen free system and circulated by means of a nitrogen gas lift pump so that any dissolved oxygen was continuously removed. A teflon cell clamped onto the reduced center section of the specimen served to contain the corrosive solution. A typical specimen with cell and extensometer mounted is shown in Fig. 1. The exposed surfaces were 0.420" x .560" areas on two opposing wide faces of flat dog-bone type specimens. The solution, a 3% NaCl solution, buffered with an addition

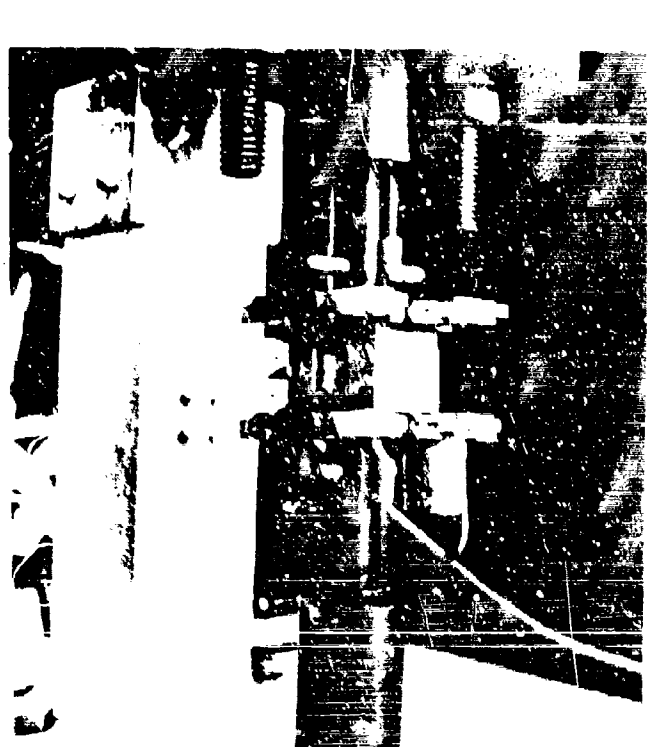

Fig. 1 Photograph of Specimen with Cell and Extensometer Mounted

of 0.5% $AlCl_3$ was circulated over one face of the specimen, then the other, then returned to the reservoir, at a rate of 120 ml/min. The pH was varied between 0.7 and 3.4 by additions of HCl to the solution; the 3.4 pH solution required no acid addition. Solution pH was checked periodically during each test and after specimen failure.

Following failure, selected specimens were sectioned in a plane parallel to the tensile axis (defined by the short transverse and longitudinal directions), then metallographically polished to reveal the crack morphology.

Results

Overall Susceptibility as a Function of pH

The time-to-failure (TTF) results as a function of pH for specimens with three different grain boundary microstructures i.e., PFZ width and grain boundary interparticle spacing are shown in Fig. 2. Considering the scatter in the data, there is only a slight difference in behavior between the AR and LNQ specimens up to a pH of 1.5. Within this range the TTF is highly dependent on pH changing by a factor of ~ 50. At pH > 1.5, the two curves diverge and the LNQ specimens fail in approximately 1/3 the time of the AR specimens. Above pH = 2.0, there is no apparent dependence on pH.

During the course of testing, the pH of the solution environment increased for exposures of greater than 10,000 minute duration. The extent of this increase was to approach a pH of 3.4. This was the pH of the buffered chloride test solution prior to HCl addition. During the course of the extended exposure, a great deal of cathodic hydrogen reduction is likely taking place. No change from the initial pH was observed for tests of shorter lifetimes. Increase in pH would be expected to prolong TTF; this is opposite to the behavior shown in Fig. 2 for the AR and LNQ materials. Therefore, the decrease in slope at higher pH does not appear to be a result of this experimental irregularity.

As can be seen from Fig. 2, the WQ specimens are less susceptible to stress corrosion than the AR and LNQ specimens at pH $\leq$ 1.3 and more susceptible for pH $\geq$ 1.5. Thus at pH of approximately 1.3, the three different grain

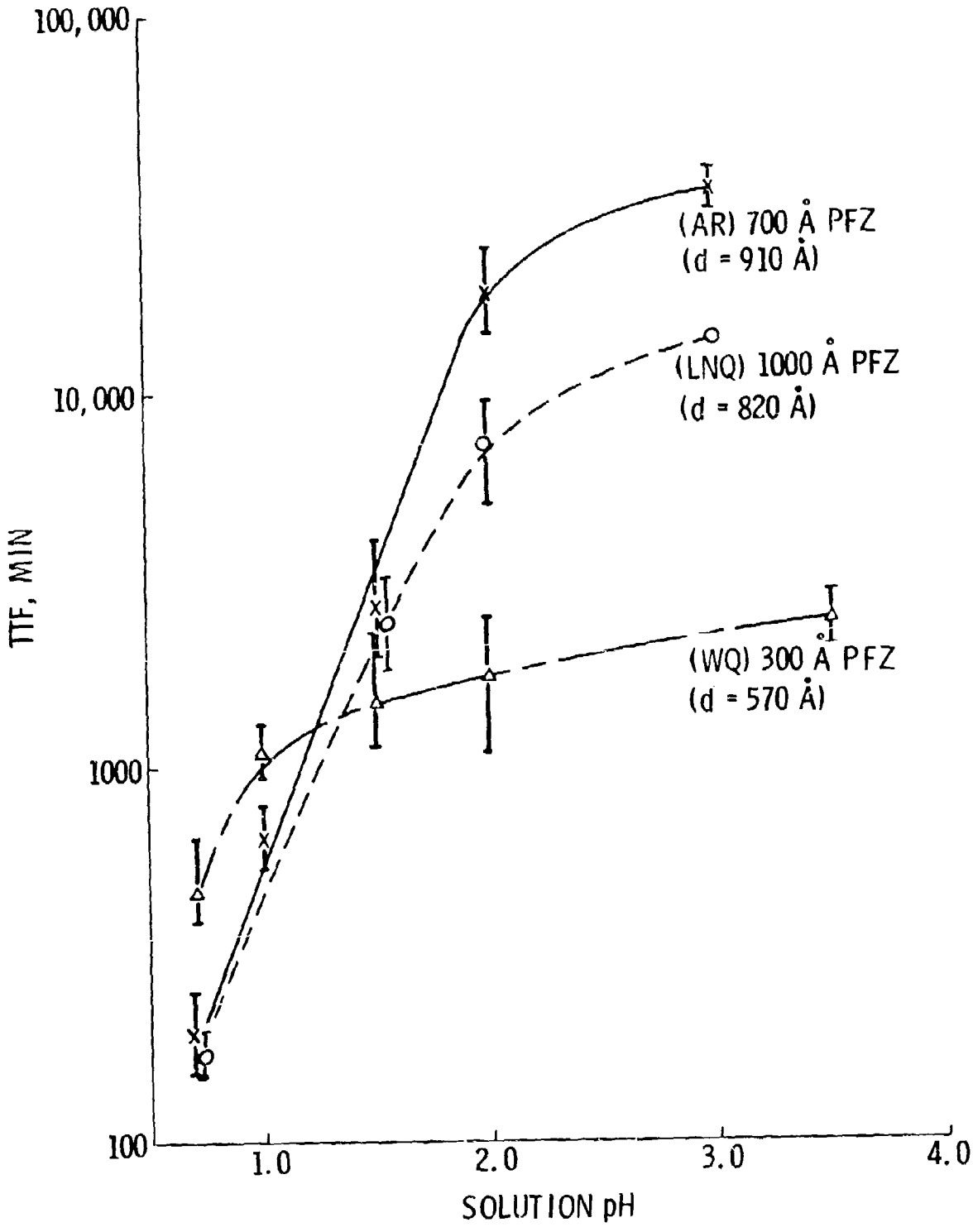

Fig. 2 Log TTF Versus pH for AR, LNQ, and WQ Materials

boundary microstructures are equally susceptible. For WQ specimens, the TTF appears dependent on pH only over the 0.7 to 1.0 range. This is in agreement with the observation of Sedricks et. al (Ref. 7, 8) who found no pH dependence over the 1.0 to 6.2 pH range for a similarly water quenched Al-Mg-Zn alloy.

The TTF results for the overaged 7075-T7351 are shown in Fig. 3 for solution pH $\leq$ 2.0. The pH dependent behavior is similar to that of the AR and LNQ specimens, although the TTF is longer at equivalent pH. Evaluation at pH > 2 for T7351 material is still under investigation due to the long times to failure at the designated stress level of this study.

Attack Morphology

Use of a smooth surface specimen allows both the initiation and propagation of attack to precede in an unrestricted manner. The morphology associated with such attack was examined in selected specimens following failure. Some observations were also made on specimens that were not stressed but exposed to the corrosive environment in the testing apparatus. Particular attention was paid to the structure of the original surface, the root of the advancing crack, and the crack width. Table II summarizes the cracking morphology as a function of pH.

At pH = 0.7, there is little difference in the crack features between the AR, LNQ and WQ specimens as shown in Fig. 4. (The attack morphology in AR and LNQ specimens are very similar so that only the AR is shown). There is only slight localized surface attack; the cracks are hairline in nature and generally extend through 50% or more of the specimen thickness. The WQ specimens have an additional feature, crack broadening at or near the surface. This dissolution at the walls of cracks is likely a result of the appreciably longer exposure times at this pH.

Both the AR and LNQ specimens show crack branching at pH = 0.7 as can be seen in Fig. 5. The smallest grain size in this material is about 90 microns (Ref. 12) and the attacked regions in Fig. 5 are only about 10 microns; therefore,

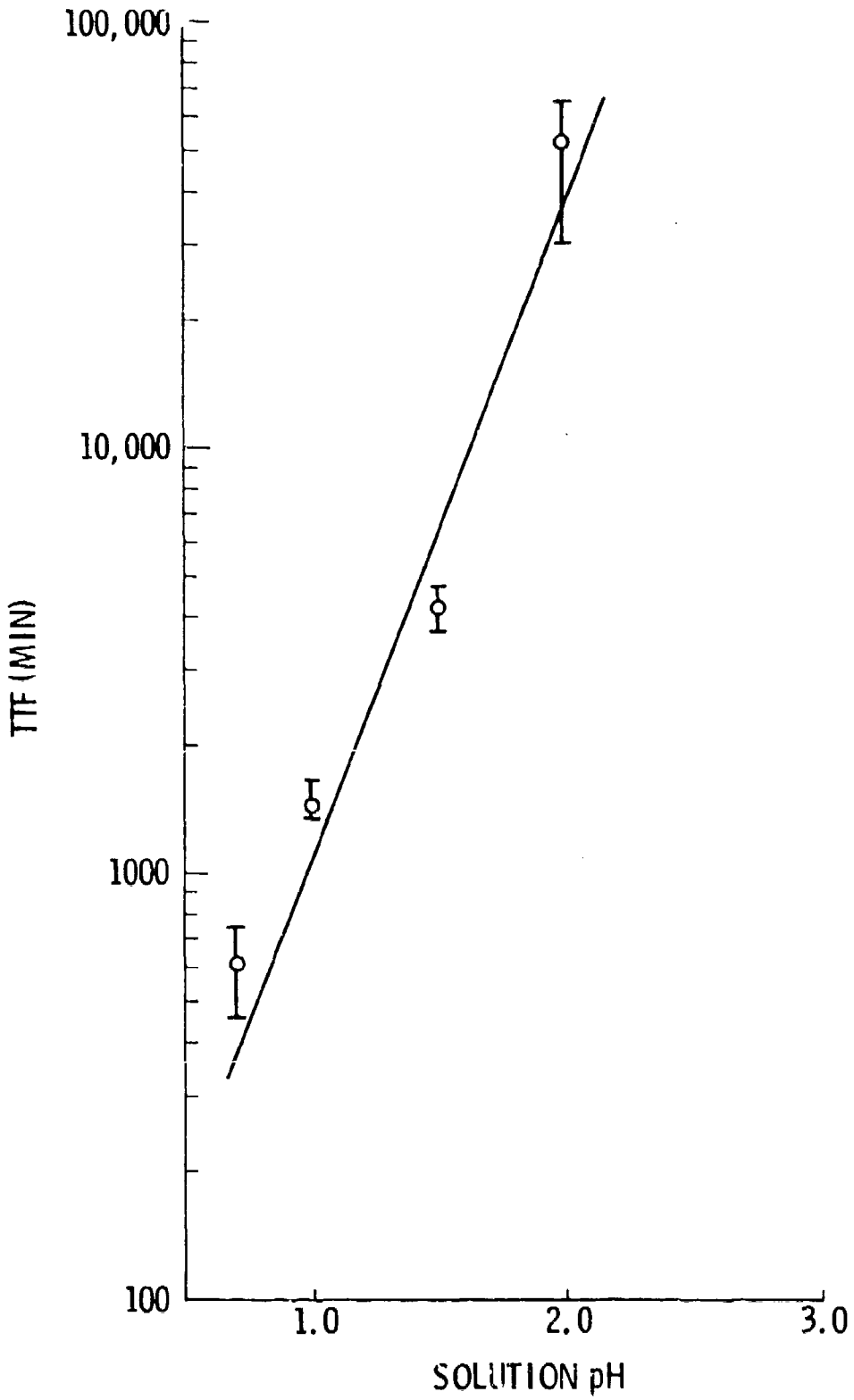

Fig. 3 Log TTF Versus pH for -T7351 AR

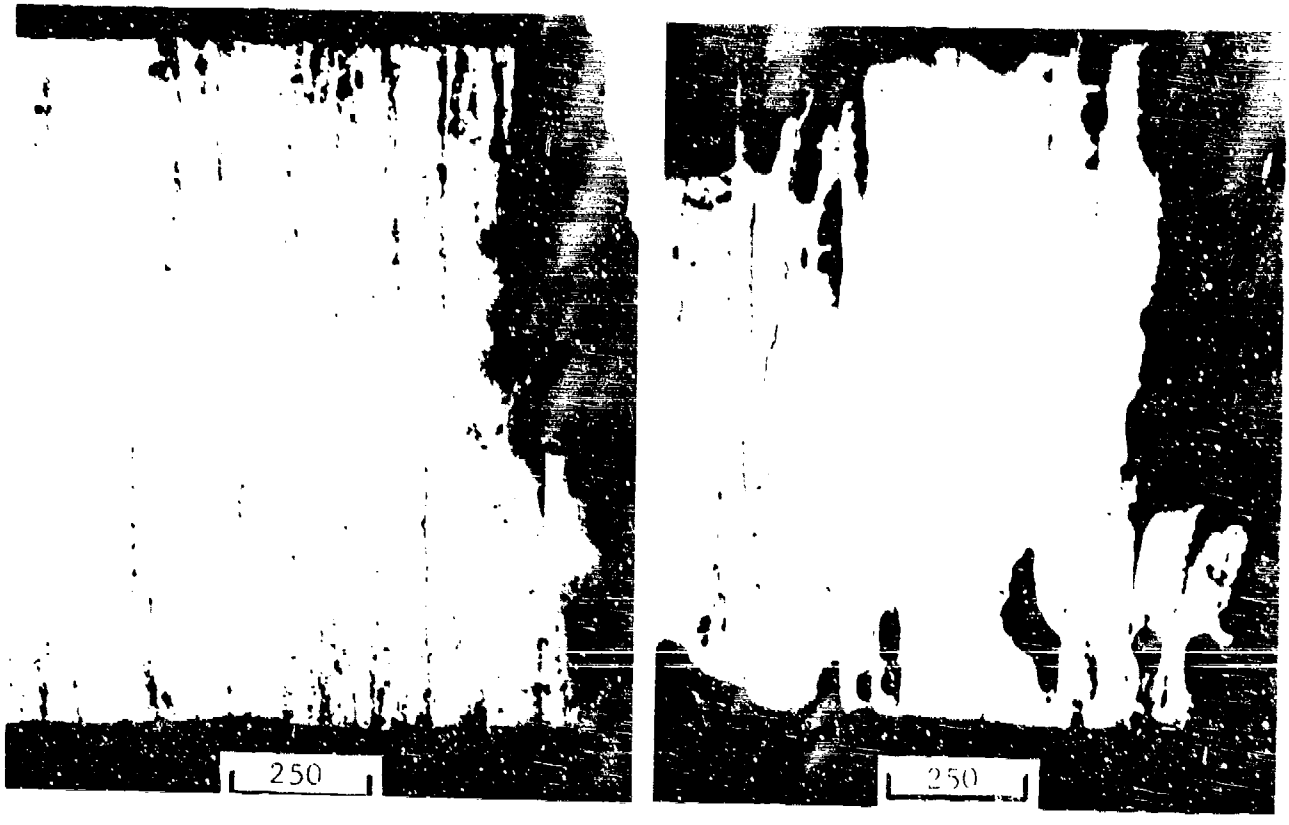

Fig. 4 Photomicrographs of Cracking in AR and WQ Specimens at a pH = 0.7 (75X)

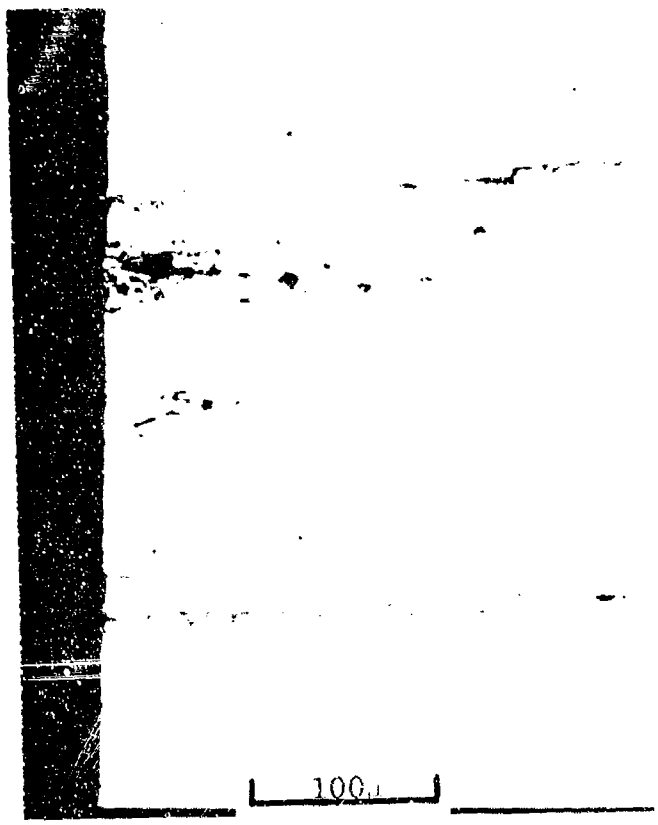

Fig. 5 Photomicrograph of Cracking Showing Branching at a pH = 0.7 in AR Specimen (250X)

branching most likely takes place along subgrain boundaries. The existence of subsurface holes also can be seen in Fig. 5; they may originate by branching and be a result of complete removal of subgrains into the flowing solution. However, internal holes were also apparent in the WQ specimens, but careful examination of many specimens did not reveal indication of branching.

Over the pH range 1.0 to 2.0, the AR and LNQ specimens continue to exhibit similar behavior, characterized in Fig. 6. There is increasing surface attack, crack broadening and blunting. At pH = 2.0, surface attack in AR specimens is more severe than in LNQ specimens. This reflects the $\sim 2\ 1/2$ times longer exposure times for the AR specimens at this pH. Evidence of sharp cracks emanating from the front of blunted areas can still be seen at pH of 2.0 (see Fig. 7).

For WQ specimens over this same 1.0 to 2.0 pH range, the extent of the attack decreases while the type of attack remains unchanged from what was observed at a pH = 0.7. This can be seen for the WQ specimens in Fig. 6. The decreasing attack of the WQ specimens in this range is in sharp contrast with the much greater degree of attack observed in the AR and LNQ at a pH = 1.5 to 2.0. These differences probably reflect the differences in the TTF in this pH range as shown in Fig. 2.

Over a pH range 2.0 to 3.0 the extent of attack decreased for all three specimens. The AR specimen, having the longest exposure had the most severe surface attack (see Fig. 8); the WQ specimen had the least. For the WQ specimen at pH of 3.4, there was almost no surface attack and only one or two sharp cracks formed (see Fig. 8). The nature of the attack on the AR and LNQ specimens, i.e., sidewise broadening and blunting remains the same over the pH range ~ 2.0 to 3.4, reflecting the relatively small changes in TTF with pH.

To observe only corrosion effects on crack morphology, a series of AR specimens were exposed at pH = 0.7, 1.5 and 3.2. (X-ray residual stress measurements on these specimens showed no appreciable stresses at the surface). In the pH = 0.7 environment, attack begins by cracking at subgrain

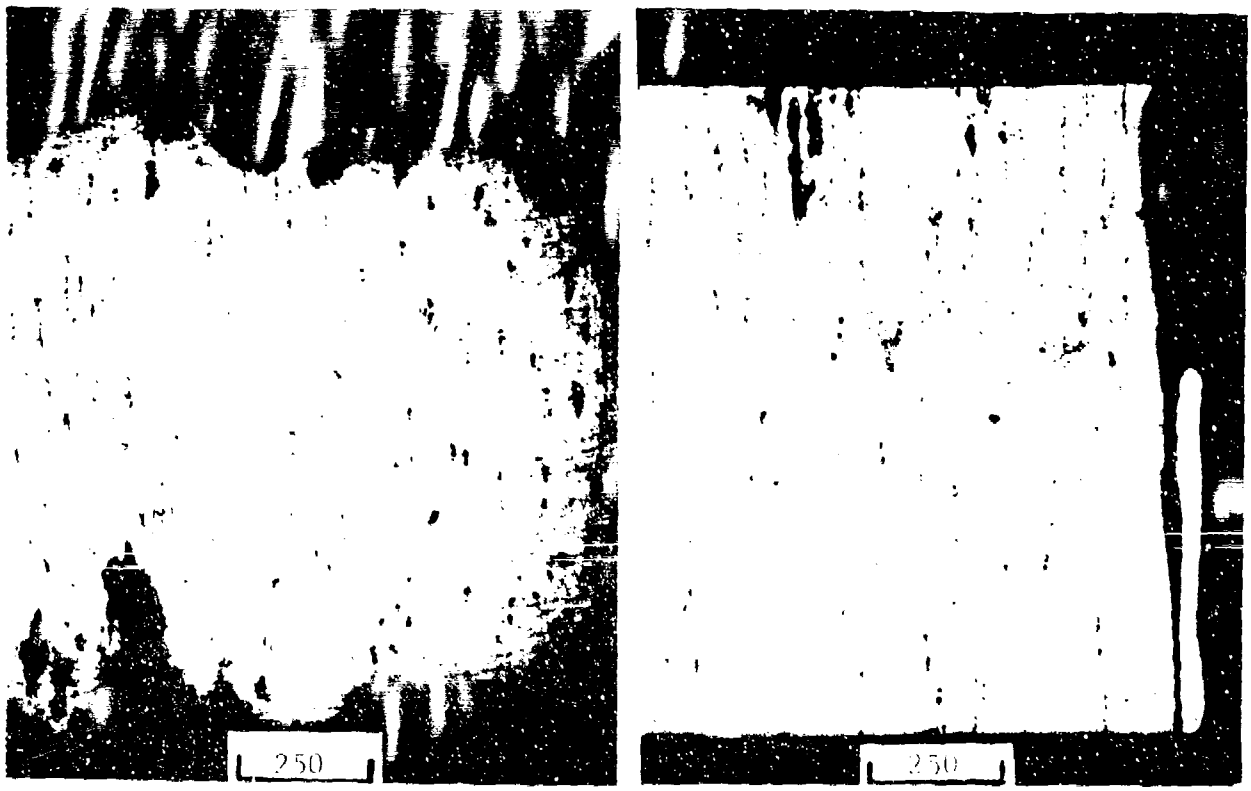

Fig. 6 Photomicrographs of Cracking at a pH = 1.5 (75X)
a) AR, b) WQ

Fig. 7 Photomicrograph Showing Sharp Crack Extending from Root of Blunt Crack at pH = 2.0 in AR Specimen (450X)

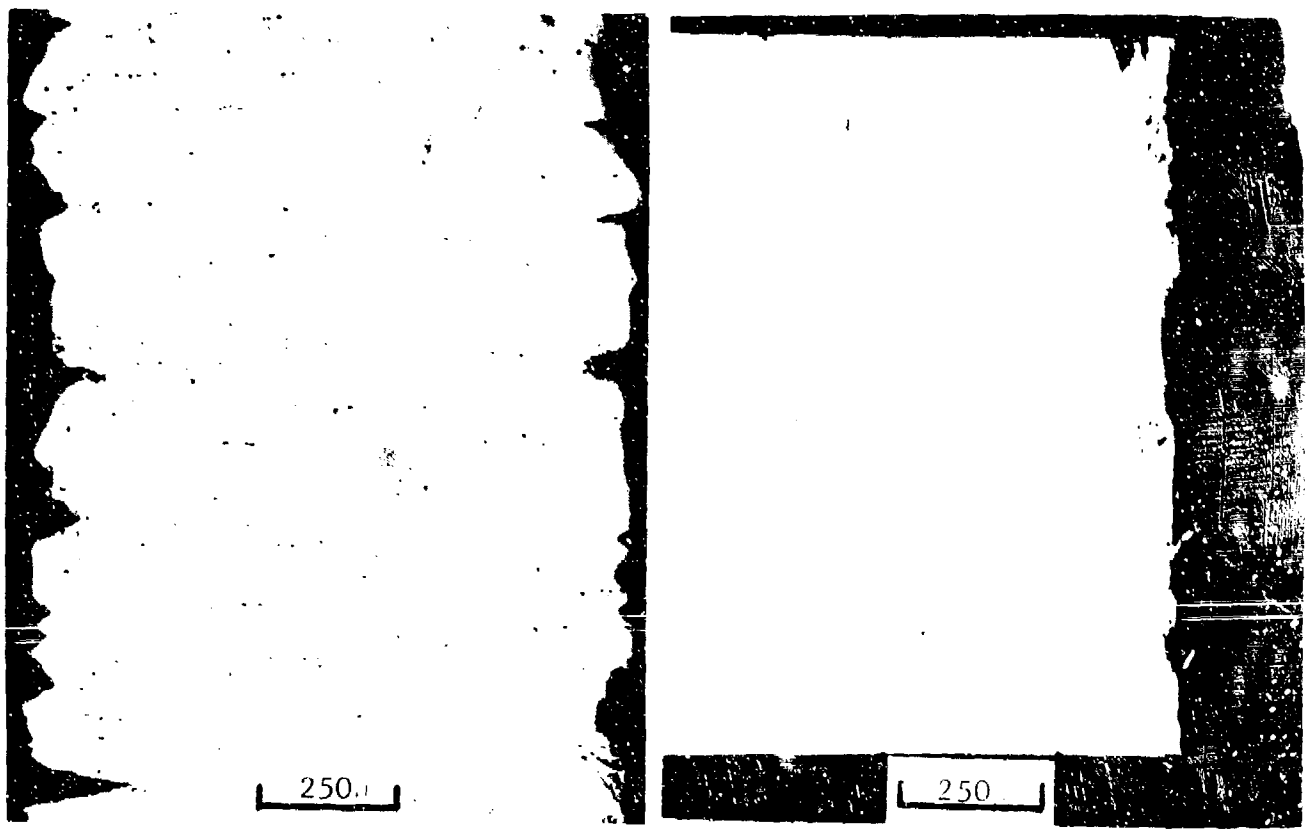

Fig. 8 Photomicrographs Showing the Nature of Attack at High pH (75X). a) AR at pH = 3.0, b) WQ at pH = 3.4

TABLE I

MICROSTRUCTURAL FEATURES OF 7075 ALLOY TEMPERS

SPECIMEN	MATRIX PRECIPITATE	PFZ WIDTH (Å)	G.B. PARTICLE SIZE (Å)	G.B. INTERPARTICLE SPACING (Å)
-T651, As Received (AR)	G.P. Zones (~ 75 Å)+ η' (~ 150 Å)	700	320 ± 110	910
Water Quenched (WQ)	G.P. Zones (~ 75 Å)+ η' (~ 125 Å)	300	270 ± 120	570
Liquid N_2 Quenched (LNQ)	G.P. Zones (~ 75 Å)+ η' (~ 125 Å)	1000	450 ± 230	820
-T7351, As Received	η' (100-300 Å)+ η (400-800 Å)	750	980 ± 310	1410

where η' - semicoherent intermediate $MgZn_2$ phase

η - incoherent equilibrium $MgZn_2$ phase

boundaries (see Fig. 9a). After 1000 minutes exposure (Fig. 9b), the attack is much more severe and is marked by a recession of the surface, a large amount of intergranular corrosion, and the formation of subsurface holes. This specimen was exposed five times longer than the average TTF (180 minutes) for stressed AR material at this pH.

Increasing the pH to 1.5 and the time to 4600 minutes (about twice the TTF for stressed specimens), produced highly localized attack (see Fig. 10). Some cracks appear to be blunted, and there is also crack broadening. Comparison with the unstressed T651 AR specimen at failure (Fig. 6) shows the attack to be more localized and deeper for the unstressed specimen. In both cases, intergranular cracks, similar to that shown in Fig. 7, were observed at the root of the broadened cracks. However, in the unstressed specimens these intergranular cracks also appeared blunted and showed some degree of broadening.

In an unstressed specimen exposed for 4200 minutes (about 12% of TTF) at a pH = 3.2, there is no evidence of localized cracking, but some slight surface pitting is apparent (see Fig. 10). Examination at higher magnification revealed a general surface dissolution to a depth of 10 to 20 microns.

Examination of the 7075-T7351 specimens in the AR condition indicated that failure was a result of mechanical overload, accompanying reduction in cross-sectional area. In the pH range 0.7 to 1.5, the attack is very general, with a reduction in specimen thickness varying from 60% at pH = 0.7 to 40% at a pH = 1.5 (see Fig. 11). For pH $>$ 1.5, there is some indication of more localized attack, but general dissolution is still extensive and accounts for an approximate 30% reduction in thickness. The localized nature of the attack at higher pH is indicated in Fig. 11. It is probable that failure at these pH levels is due to this localized attack since there is only slight overall surface reduction.

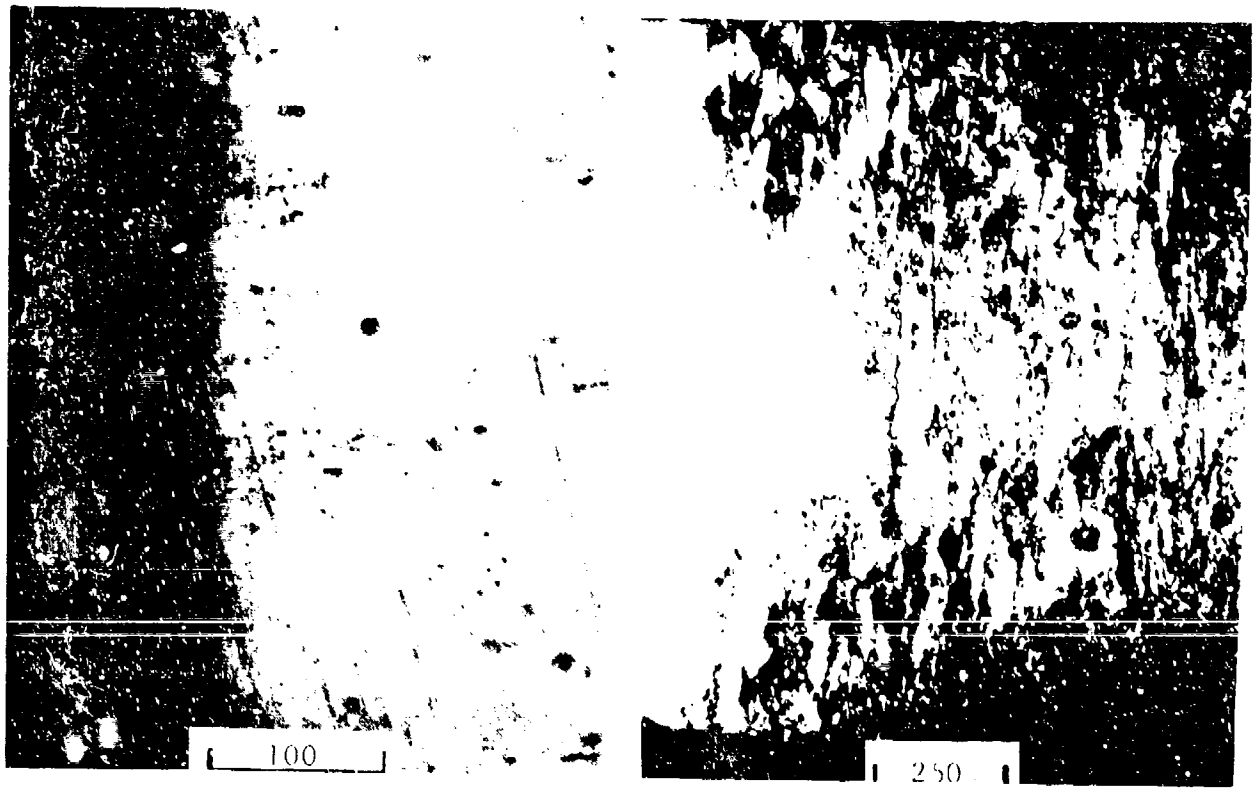

Fig. 9 Photomicrographs Showing the Effect of Time on the Corrosion of Unstressed AR Specimens at a pH = 0.7. a) 45 Minutes (250X), b) 1000 Minutes (75X)

TABLE II

CRACK MORPHOLOGY

pH	Type of Attack at Failure				
	T651, AR	LNQ	WQ	T7351, AR	T651, Unstressed*
0.7	sharp, intergranular attack	sharp, intergranular attack	sharp, intergranular attack; crack broadening near surface	general attack	subgrain attack; sharp, intergranular attack; surface recession
1.0	increased crack broadening and blunting; increasing surface attack	increased crack broadening and blunting; increasing surface attack	decreasing surface attack		
1.5				localized attack	sharp, intergranular attack; some crack broadening
2.0	crack broadening and blunting; decreasing surface attack	crack broadening and blunting; decreasing surface attack			
2.5					
3.0					
3.4					surface pitting; general attack

* No failures observed

Discussion

To explain the characteristics observed in these studies, we will first consider the cases of pH dependent and independent susceptibility, individually, and then the transition of one to the other.

1) pH Dependent Susceptibility

Change in TTF as a function of pH occurs for all four tempers illustrated in Figs. 2 and 3; however, the pH range over which dependence exists differs. There is only a limited range over which the WQ material shows dependence on pH, whereas the other three tempers have a range that extends from pH 0.7 at least 2.0. Sedricks et al (Ref. 8) have shown that lowering of pH below 4 promotes anodic dissolution by enhancement of the cathodic hydrogen ion reduction process for an alloy and solution environment similar to those used in the present work. Hence, the pH dependence in Figs. 2 and 3 may be attributable to enhancement of anodic dissolution at lower pH. This is consistent with the general attack mode shown in Fig. 11 for the AR T7351 temper as well as the severe surface attack at low pH shown in Figs. 4, 6, and 9 for AR and WQ material.

An additional mode of attack, that of sharp intergranular cracking is evident for AR and WQ materials over the pH dependent susceptibility range, as can be seen in Figs. 4, 6 and 7. This type of localized attack at grain boundaries also occurs in unstressed AR samples, see Figs. 9 and 10, and is apparently effective in causing branching at subgrain boundaries, see Fig. 5. It is likely that the difference in chemistry between the boundaries and matrix (Ref. 13) in the highest strength temper material leads to differences in electrochemical potential between the two which promotes the observed dissolution behavior. The existence of long cracks that propagate at a rate dependent on pH as shown in Fig. 12 (earlier work (Ref. 1) showed that the TTF results reflect the crack propagation stage, tp, of stress corrosion attack) indicates that the stress corrosion model suggested by Sedricks et al (Ref. 8) is not applicable here. This model proposes that cracking rate is relatively

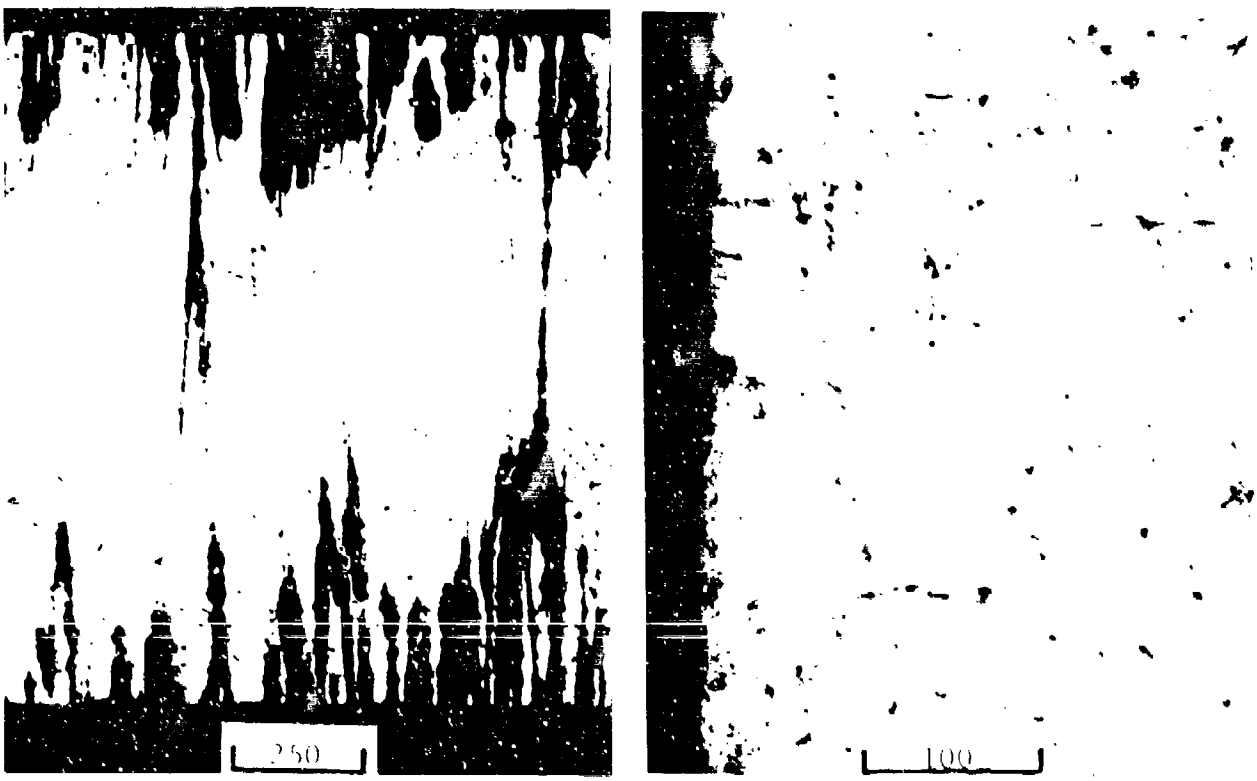

Fig. 10 Photomicrographs Showing the Effect of Corrosion on Unstressed AR Specimens. a) pH = 1.5, 4600 Minutes (75X), b) pH = 3.2, 4200 Minutes (250X)

Fig. 11 Photomicrographs Showing the Nature of Attack in 7075-T7351 AR Specimens (75X). a) pH = 0.7, b) pH = 1.5

independent of solution pH due to a hydrolysis region of constant pH near the tip of long cracks where much of the effective cathodic reaction occurs.

2) pH Independent Susceptibility

For the three high strength tempers (AR, LNQ and WQ) the TTF is relatively independent of pH at higher pH. The previously described hydrolysis model involving constant effective pH could be considered, but the attack morphology in two of these cases, AR and LNQ, is not consistent with this interpretation. For these two tempers, a great deal of blunting and crack widening is evident at higher pH, as shown in Figs. 7 and 8. Access by the solution to the crack front area appears readily achievable, although there is some incidence of sharp cracks near the root of blunted fronts, see Fig. 7.

In any case, the crack propagation rate for AR and LNQ materials is much smaller than for WQ material as shown by the differences in tp in Fig. 12. While blunting and crack widening occur at higher pH for AR and LNQ material, cracking in the WQ material remains sharp and intergranular to at least pH of 3.4, see Table II. To explain this difference in attack behavior and account for the difference in propagation rates for material having essentially the same matrix microstructure but different grain boundary precipitate microstructure, we will consider the stress behavior at the grain boundary of this material.

For a simple case of two discs embedded in a matrix, let us consider the effect of a constant overall displacement. If we assume that the discs and the matrix have the same elastic modulus, the stresses in the discs and matrix will be the same as long as the displacement is linearly elastic. However, if the matrix is ductile with a relatively low yield strength while the discs are brittle, the stresses in these materials will not be the same at constant displacement once yielding in the matrix takes place. The stress increases in the brittle discs by a greater amount than that accompanying work hardening in the matrix. As the strain increases, one of the discs will reach its

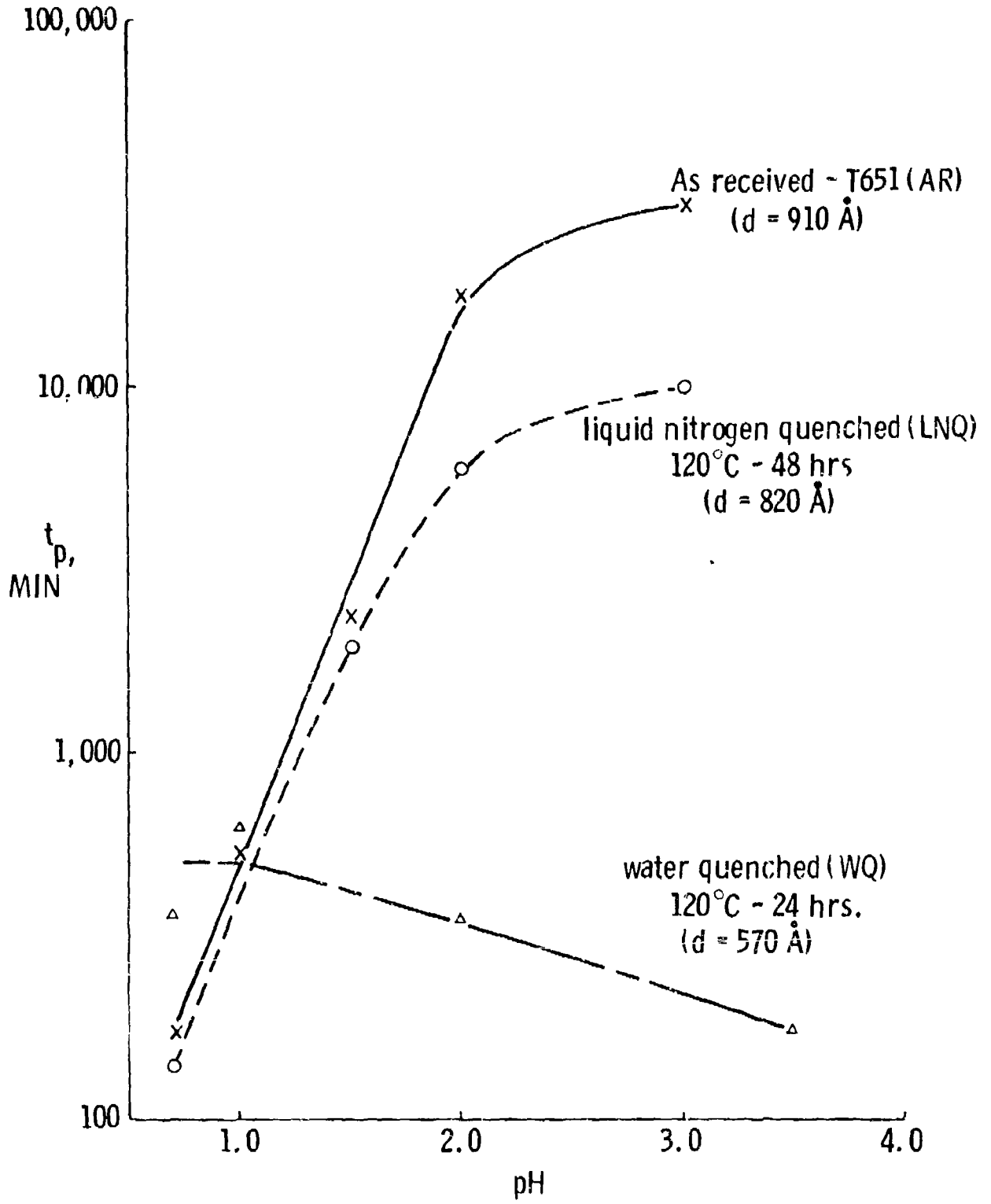

Fig. 12 Time for Cracks to Propagate (tp) as a Function of pH for AR, LNQ, and WQ Specimens

fracture stress. At this point, the matrix must accommodate the additional stress in a manner analogous to that associated with a solid containing a"penny shaped"crack. The ability to accommodate the additional stress is a function of the distance between discs. If accommodation is possible, the crack will not propagate readily. However, if the distance between discs is too small, stress will concentrate and lead to cracking in adjacent discs and continued crack propagation. More quantitative details concerning the extent of stress concentration and effect of distance and size are under consideration.

For grain boundary attack in 7075, the precipitate-free-zone (PFZ) adjacent to nigh angle boundaries can be considered as the matrix in this model and $MgZn_2$ grain boundary precipitate particles as the discs. Tilted stage transmission electron micrographs of this alloy (Ref. 1) show that this characterization represents the microstructure in the vicinity of a grain boundary. Both materials have approximately the same elastic modulus (Ref. 14). The aluminum solid solution of the PFZ could be considered as ductile relative to the $MgZn_2$ intermetallic precipitate. Therefore, increased grain boundary precipitate spacing would act to reduce the rate of crack propagation at grain boundaries. This is evident from the curves in Fig. 2 where the WQ material of shortest interparticle spacing, d, fails in the shortest times. The attack morphologies in these materials at higher pH is also consistent with this model.

3) Transition from pH Dependent to pH Independent Susceptibility

Two modes of stress corrosion attack have been described in parts (1) and (2) of this discussion. For the first, attack appears dependent on a dissolution mechanism. This is promoted by hydrogen ion reduction at cathodic areas. Both localized and general attack modes are observed; applied stress appears more effective in the propagation of localized, grain boundary attack. The second mode requires the presence of the environment to reduce the stress intensity at which cracks will propagate and is controlled by the stress concentration at grain boundaries. Grain boundary precipitate microstructure, specifically the precipitate spacing, is

primarily significant to the crack propagation rate. Material having short grain boundary precipitate spacing act to concentrate stress and propagate cracks whereas blunting occurs for larger spacings.

At low pH, the dissolution dependent mechanism of attack is most effective as evidenced by pH dependent behavior for all the tempers examined over the 0.7 to 1.0 pH range. Transition to the stress concentration mechanism occurs when this mode can cause cracks to propagate more readily than by dissolution. This occurs above the relatively low pH of 1.0 for WQ material with 570 Å interparticle spacing. It does not occur until above pH 2.0 for the LNQ and WQ materials of 820 and 910 Å spacing, respectively. It is unlikely that the large interparticle spacing of 1410 Å for AR T7351 will allow the stress concentration mechanism to operate.

Acknowledgments

We would like to acknowledge the continuing efforts of William Poit, Vince Murtha and Cal Lottermoser on the experimental portion of this work, and thank Drs. Ernesto Saleme and Harry Armen for their help in setting up the grain boundary model.

References

1. P.N. Adler, R. DeIasi and G. Geschwind, to be published in Met. Trans., Dec. 1972.

2. B.F. Brown, C.T. Fujii and E.P. Dahlberg, J. Electrochem. Soc., 116, 218, (1969).

3. J.A. Davis, Use of Microelectrodes for the Study of Stress Corrosion of Aluminum Alloys, Bell Aerospace Co. Report, Oct. 1971.

4. K.G. Kent, J. Aust. Inst. Met., 15, 171, (1970).

5. K.G. Kent, J. Inst. Met., 97, 127, (1969).

6. P.N.T. Unwin and R.B. Nicholson, Acta. Met., 17, 1379, (1969).

7. A.J. Sedricks, P.W. Slattery and E.N. Pugh, Trans. ASM, 62, 238, (1969).

8. A.J. Sedricks, J.A.S. Green and D.L. Novak, Met. Trans., 1, 1815, (1970).

9. Alcoa Aluminum Handbook, Aluminum Co. of America, (1967).

10. G. Geschwind, G.C. Soltz and P.N. Adler, Corrosion, 26, 165, (1970).

11. D.O. Sprowls and R.H. Brown, Fundamental Aspects of Stress Corrosion Cracking, NACE, (1969).

12. P.N. Adler, R. DeIasi, C.H. Li and G. Geschwind, Two Stage Mechanism of Stress Corrosion Attack in High Strength Aluminum Alloys, presented at the Fall Meeting TMS Cleveland, Ohio, (1970). To be published.

References (Continued)

13. S.B. Brummer, et. al, Study of the General Mechanism of Stress Corrosion of Aluminum Alloys and Development of Techniques for its Detection, Tyco Laboratories, 2nd Annual Report on Contract NAS 8-20297, (1968).

14. L. Guillet and R. LeRoux, "Elastic Behavior", p. 456 in Intermetallic Compounds, ed. by J.H. Westbrook, John Wiley and Sons, N.Y. (1967).